Chinese Journal of Mechanical Engineering

ORIGINAL ARTICLE

Open Access

Discrete Optimization on Unsteady Pressure Fluctuation of a Centrifugal Pump Using ANN and Modified GA

Wenjie Wang[1], Qifan Deng[1], Ji Pei[1*], Jinwei Chen[1,2] and Xingcheng Gan[1]

Abstract

Pressure fluctuation due to rotor-stator interaction in turbomachinery is unavoidable, inducing strong vibration in the equipment and shortening its lifecycle. The investigation of optimization methods for an industrial centrifugal pump was carried out to reduce the intensity of pressure fluctuation to extend the lifecycle of these devices. Considering the time-consuming transient simulation of unsteady pressure, a novel optimization strategy was proposed by discretizing design variables and genetic algorithm. Four highly related design parameters were chosen, and 40 transient sample cases were generated and simulated using an automatic program. 70% of them were used for training the surrogate model, and the others were for verifying the accuracy of the surrogate model. Furthermore, a modified discrete genetic algorithm (MDGA) was proposed to reduce the optimization cost owing to transient numerical simulation. For the benchmark test, the proposed MDGA showed a great advantage over the original genetic algorithm regarding searching speed and effectively dealt with the discrete variables by dramatically increasing the convergence rate. After optimization, the performance and stability of the inline pump were improved. The efficiency increased by more than 2.2%, and the pressure fluctuation intensity decreased by more than 20% under design condition. This research proposed an optimization method for reducing discrete transient characteristics in centrifugal pumps.

Keywords Centrifugal pump, Unsteady performance optimization, Discrete design variable, Discrete genetic algorithm

1 Introduction

Centrifugal pumps are widely used in irrigation, petroleum, chemicals, and nuclear power as the core of fluid transport. A vertical inline pump is a special type of centrifugal pump with an elbow-shaped inlet structure. It is widely utilized to solve limited installation space, such as urban water supply and ship transportation [1]. However, the curved inlet channel deteriorates the inflow condition, which decreases the hydraulic performance and increases the risk of damage. Pressure fluctuation is one significant factor that affects the pump's operation stability and efficiency. Pressure fluctuation increases vibration and cannot be eliminated, even under the design condition [2, 3]. Therefore, finding the optimal design balancing both the reduction in pressure fluctuation and increasing energy savings is significant.

Many researchers have tried to reduce pressure fluctuation in centrifugal pumps. Fu et al. [4] investigated the influence of the stagger angle of a double-entry impeller on pressure fluctuation and found an optimized impeller arrangement. Li et al. [5] modified the leading edge shape of a pump-turbine impeller (working in pump mode) to reduce the pressure fluctuation in the hump

*Correspondence:
Ji Pei
jpei@ujs.edu.cn
[1] National Research Center of Pumps, Jiangsu University, Zhenjiang 212013, China
[2] China Energy Jiangsu Jianbi Power Co. Ltd, Zhenjiang 212006, China

region. However, the most optimal solution might not be achieved due to the limited variables and samples. Optimization with multiple parameters is necessary to reduce pressure fluctuation inside centrifugal pumps. However, optimizing pressure fluctuation reduction is still a novel topic because of the time-consuming CFD simulation process to obtain accurate pressure data. Although steady-state simulation has been popular in efficiency optimization with the advantage of time-saving, it is necessary to conduct a transient simulation to obtain a pressure fluctuation signal, and enough simulation time is also significant to improve the resolution of time and frequency, which is time-consuming. Thus, appropriate optimization methods should be selected to accelerate the optimization process. Pressure fluctuation also appears to be nonlinear and discrete. It is significant to appropriately establish the relationship between the fluctuation and the pump parameters.

Benefitting from the development of computational resources, contemporary optimization methods combining parametric design, CFD prediction, surrogate models, and intelligent algorithms are broadly applied to improve the performance of pumps. At the same time, many studies have confirmed the feasibility and stability of these approaches [6–10].

The common surrogate models used in the optimizing design of pumps include response surface model (RSM) [6, 9, 11], artificial neural network (ANN) [7, 12–14], Kriging model [8, 15], etc. The capacity of different models was tested [16], and ANN with two hidden layers was proven to have great accuracy in predicting multi-peak functions [17], which is suitable for optimizing pressure fluctuation.

On the other hand, pump optimization problems usually show great complexity and are computationally resource-intensive [18]. Therefore, improving the convergence speed of the algorithms is essential to reduce computational costs and improve optimization efficiency. Many studies have been reported to improve the algorithm performance to solve complicated optimization problems (e.g., improving cavitation performance) by modifying the existing algorithms (e.g., Genetic Algorithm [19, 20], Particle Swarm Optimization [21]). Nourbakhsh et al. [22] presented research that compared the performance of NSGA-II and MOPSO for a centrifugal pump optimization problem, which indicated that the PSO algorithm produced better results than the GA.

Genetic algorithm (GA) is a biological evolutionary model based on Charles Darwin's theory of natural selection and is widely used in signal processing, machine learning, combinatorial optimization, adaptive control, and artificial life [23]. Genetic algorithm can also be used for discrete optimization problems.

Although the efforts of many scholars have significantly improved these algorithms, their performance in solving optimization problems with large computational volumes is still unsatisfactory. Thus, current pump optimization schemes mainly focus on improving efficiency, head, and other steady characteristics [24–27]. Few studies have investigated optimizing unsteady characteristics, such as pressure fluctuation intensity, due to the enormous computation requirements. Other than increasing computational resources, the best way to improve optimization is to reduce the sample quantity requirements for this situation. Two aspects are considered to reduce the optimization period: the design variables are made discrete, and a novel discrete genetic algorithm is proposed to solve the discrete optimization problems.

This research proposed a modified discrete genetic algorithm (MDGA) based on the classic genetic algorithm with a binary encoding of discrete fetching positions to improve convergence and search performance. The detailed modification and testing procedures are presented in Section 2.4.

In this research, the accuracy of the simulation was verified by comparing both pump performance and pressure fluctuation before and after optimization. The intensity of pressure fluctuation near the volute tongue of a vertical inline pump was considered as the optimization objective. Four design parameters of the impeller blades were selected. Meanwhile, the MDGA was proposed to reduce the sample requirements. Finally, a further comparison of the performance and flow conditions between the original and optimized cases was carried out to analyze the reasons for the observed performance improvements.

2 Methodology

2.1 Numerical Methodology

2.1.1 Computational Model

In this research, the impeller of an industrial inline pump (specific speed n_s = 132; in Chinese standard, the

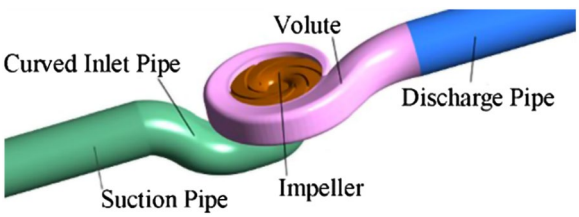

Figure 1 Computational domain

Table 1 Original geometry parameters

Parameter Name	Value
Pump inlet diameter D_s (mm)	80
Pump outlet diameter D_d (mm)	80
Impeller inlet diameter D_1 (mm)	72
Impeller outlet diameter D_2 (mm)	136
Impeller inlet width b_1 (mm)	34.5
Impeller outlet width b_2 (mm)	17.8
Impeller blade number z	6
Impeller blade angle at the leading edge β_1 (°)	38
Impeller blade angle at the trailing edge β_2 (°)	23

Table 2 Grid sensitivity analysis

Scheme index	Node number ($\times 10^6$)	Head (m)
A	0.976	20.122
B	1.126	19.698
C	1.434	19.776
D	1.817	20.185
E	2.387	20.196
F	3.482	20.245
G	4.290	20.275
H	6.603	20.281
I	8.390	20.284

definition is given as Eq. (1)) was optimized, and the characteristics of the original case, sample cases, and the optimized case were predicted using numerical simulations. As shown in Figure 1, the flow domain was divided into five parts in the CFD calculations, including the suction pipe, the curved inlet pipe, the impeller, the volute, and the discharge pipe. The design flowrate Q_d is 50 m^3/h, the design head H_d is 20 m, and the nominal rotation speed n is 2910 r/min. Other geometry parameters of the original model are listed in Table 1.

$$n_s = \frac{3.65n\sqrt{Q_d}}{H_d^{3/4}}, \tag{1}$$

where n_s is the specific speed, n is the nominal rotation speed, Q_d is the design flowrate, and H_d is the design head.

2.1.2 Grid Distribution

The grids of each domain shown in Figure 1 were generated using ANSYS ICEM CFD coupled with the multi-block strategy to improve the overall grid quality. The near-wall regions were refined to capture accurate near-wall flow behaviours, and the number of nodes in each flow passage was determined using grid sensitivity analysis.

Table 3 Grid specifications

Component	Suction Pipe	Inlet Pipe	Impeller	Volute	Discharge Pipe
Nodes number	779544	581578	933510	1216305	779544

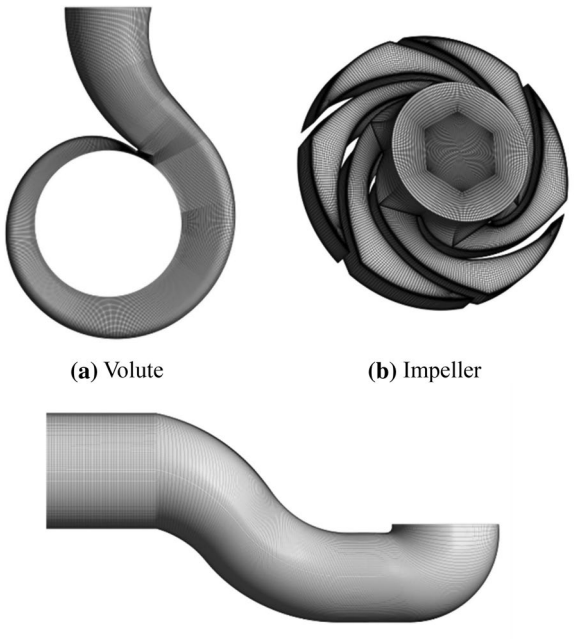

(a) Volute **(b)** Impeller

(c) Curved inlet pipe

Figure 2 Grid condition: **a** Volute, **b** Impeller, **c** Curved inlet pipe

The test results are listed in Table 2. It can be observed that the computational head was approaching stability when the grid number increased by 4.29 million, so grid scheme G was chosen for further research. The grid specifications are given in Table 3. Meanwhile, the maximum $y+$ for the whole flow domain is less than 30, and the figure for crucial areas such as the leading edge and the tongue was less than 10, which met the requirement of flow feature predictions in the pump by using the shear stress transport k-ω turbulence model (SST) [28, 29]. The final grid conditions are shown in Figure 2.

2.1.3 Numerical Setup

In this research, the three-dimensional Unsteady Reynolds-averaged Navier–Stokes equations were solved by the commercial CFD code ANSYS CFX coupled with the SST k-ω turbulence model for the flow predictions.

The boundary conditions were set in accordance with the actual working conditions. Specifically, the

total pressure inlet with the value of 1 atm and the mass flowrate outlet were used to describe the pump outlet. All physical surfaces in the flow domains were set as no-slip walls with a roughness of 25 μm. The solution under steady state was first conducted with the "Frozen Rotor" strategy for interfaces between the rotors and stators. The result was utilized as the initial situation for transient computation. For the transient cases, the interfaces between the rotors and stators were changed to the "Transient Rotor–stator. Thus the relative position between the impeller and the volute was updated at each timestep [29]. The timestep in the transient cases was set as 1.718×10^{-4} s, the time required for the impeller to rotate by 3 degrees. The typical time duration is 0.5155 s, corresponding to the time it takes to perform 25 rotations. The average mathematical value of each variable of the last rotation was used to describe pump performance, and the pressure data from the last 15 rotations (0.2062– 0.5155 s) were selected for the pressure fluctuation analysis.

Furthermore, in order to evaluate the pressure fluctuation intensity, a dimensionless pressure fluctuation intensity coefficient (PFIC) was defined in Eq. (2). A monitor point V1 was added to obtain the pressure fluctuation features near the tongue (as shown in Figure 3).

$$C_p^* = \frac{\sqrt{\frac{1}{N}\sum_{j=0}^{N-1}\tilde{p}\left(node,\, t_0+j\Delta t\right)^2}}{\rho u_2^2/2}, \tag{2}$$

where, N is the number of pressure samples, $\tilde{p}$ is the periodic pressure component, *node* is the grid node index, t_0 is the start of the rotation period, ρ is the fluid density, and u_2 is the circumferential velocity at the impeller outlet.

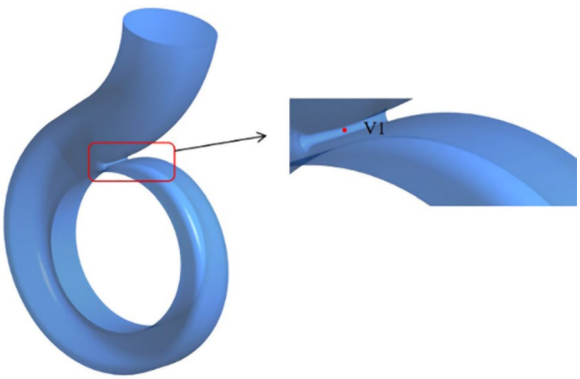

Figure 3 Location of monitor point at volute tongue

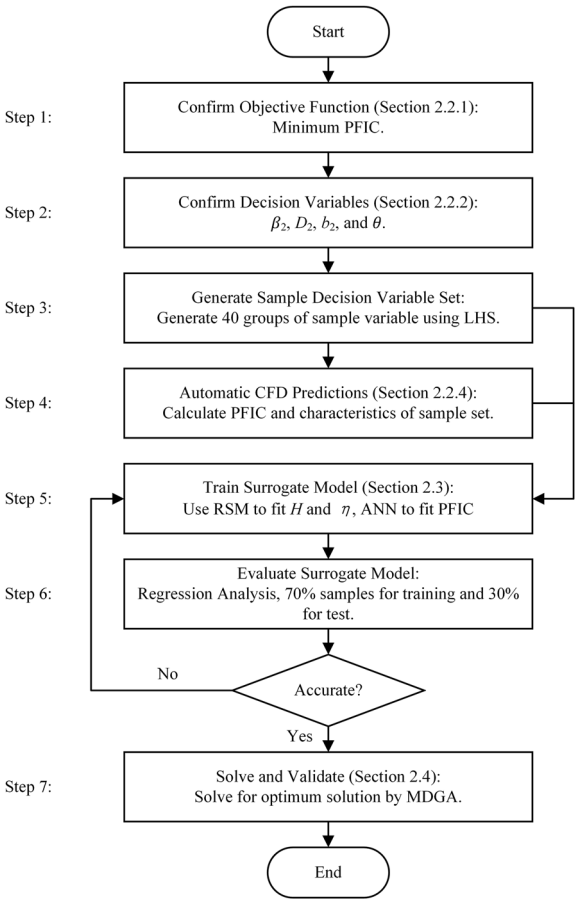

Figure 4 Optimization procedure

2.2 Optimization Procedure

The overall optimization procedure for the inline pump is shown in Figure 4, which can be classified into four main parts: optimization problem definition (Step 1 and Step 2), sample data set generation (Step 3 and Step 4), surrogate model training (Step 5 and Step 6), and solving the model (Step 7).

The optimization process based on transient sample cases requires a lot of computational resources and time. Therefore, two approaches were applied in this study to reduce the sample size requirements. Firstly, it is well-known that the accuracy of surrogate models is highly related to the used samples, and the required sample size is related to the number of variables [18]. Hence, in Step 2, a data mining process was carried out to select highly correlated variables, and four decision variables were chosen for the optimization process. On the other hand, the pump optimization problem does not require high convergence precision because the model's precision is limited, and more iterations mean higher computational costs. Thus, to fix this situation,

a modified discrete genetic algorithm was proposed in Step 7 to achieve a fast convergence performance.

2.2.1 Objective Function

In order to improve both efficiency and operating reliability of the inline pump, minimizing the pressure fluctuation coefficient under the nominal condition was considered the objective function. On the other hand, the efficiency and the head were utilized as the constraints through the optimization process to prevent drops in performance. The mathematical description of the objective function is given in the Eq. (3):

$$\begin{aligned} &\min(C_{p,1.0Q_d}^{V1}),\\ &\text{subject to}\begin{cases} \eta_{1.0Q_d}^{OPT} > \eta_{1.0Q_d}^{ORI},\\ H_{1.0Q_d}^{OPT} \geq 0.90H_{1.0Q_d}^{ORI}, \end{cases} \end{aligned} \tag{3}$$

where C_p^{V1} is the PFIC at the monitor V1 (Eq. (2) and Figure 3), η is the efficiency, and H is the head. The superscripts OPT and ORI represent the cases generated during the optimization process and the original case, respectively. The subscript $1.0Q_d$ indicates the nominal condition.

2.2.2 Decision Variables

This research aims to improve the stability and unsteady performance of an inline pump. The impeller is the only energy conversion component in the pump and has the greatest impact on performance. Therefore, four design variables of the impeller were chosen as the decision variables through the data mining process; their ranges are listed in Table 4.

Table 4 Decision variables and boundaries

Parameter	Range
Blade angle at trailing edge β_2(°)	[20, 40]
Impeller outlet diameter D_2(mm)	[128, 134]
Impeller outlet width b_2(mm)	[15, 20]
Blade wrapping angle θ(°)	[80, 120]

2.2.3 Automatic Simulation Technique

An automatic simulation program for the inline pump was proposed based on MATLAB code and ANSYS WorkBench. The geometries of the impeller cases were generated using ANSYS BladeGen parametrically and then meshed using ANSYS TurboGrid. Finally, the CFD cases were created and calculated using ANSYS CFX [7].

2.2.4 Design of Experiment

We used the Latin hypercube sampling (LHS) method for sampling, and 40 sets of valid design samples were selected in the discrete variable decision space. The performance data and pressure fluctuation intensity obtained by unsteady simulation are shown in Table 5.

2.3 Surrogate Model

2.3.1 Response Surface Model

The response surface model (RSM) combines experimental design and mathematical modelling. The model can fit the mathematical relationship between the target value and the design variables through fewer trials and construct the equation between the optimization target and the design variables so that the approximate model is closer to the real functional relationship between them [30]. Many studies also report that the RSM method performs well in predicting the characteristics of pumps such as efficiency and head [6, 9].

In this research, the RSM method was applied to fit the relationship between the external characteristics and the

Table 5 Sampling data and simulated results

NO	β_2(°)	D_2(mm)	b_2(mm)	θ(°)	η_y(%)	H (m)	Cp*
1	32	131	19	80	79.48	22.11	0.1829
2	36	133	16	110	82.76	22.11	0.0946
3	24	129	20	115	83.44	20.68	0.1419
4	36	128	18	105	84.41	21.12	0.0531
5	28	132	16	105	82.36	21.00	0.1030
…	…	…	…	…	…	…	…
36	40	133	17	90	81.48	22.71	0.1171
37	28	129	19	100	81.88	20.91	0.1115
38	28	134	15	110	82.53	21.55	0.0828
39	32	130	15	85	80.83	20.43	0.1652
40	40	128	17	95	83.59	21.11	0.1445

decision variables (Section 2.2.2), and the final prediction functions are given in Eqs. (4) and (5):

$$\begin{aligned}\eta =& -326.48+2.22\beta_2+4.65D_2+4.03b_2+0.99\theta\\ &-0.0086\beta_2^2-0.0147D_2^2-0.0691b_2^2-0.0015\theta^2\\ &-0.0096\beta_2D_2-0.0027\beta_2b_2-0.0029\beta_2\theta\\ &-0.0188D_2b_2-0.0047D_2\theta+0.0075b_2\theta,\end{aligned} \tag{4}$$

$$\begin{aligned}H =& 265.53+1.73\beta_2-4.49D_2-1.08b_2+0.05\theta\\ &-0.0079\beta_2^2+0.0183D_2^2-0.0002b_2^2-1.1228\theta^2\\ &-0.0060\beta_2D_2-0.0096\beta_2b_2-0.0017\beta_2\theta\\ &+0.1403D_2b_2+0.0002D_2\theta-0.0012b_2\theta.\end{aligned} \tag{5}$$

In addition, a regression analysis was carried out to evaluate the model's reliability. The sample case set was divided into two groups: 70% were used to train the model, and the other 30% were used for testing. The overall R^2 (the definition given in Eq. (6)) of these two models are 0.9502 and 0.9976, respectively. Hence, the accuracy of these two models is good enough for the predictions during the optimization process.

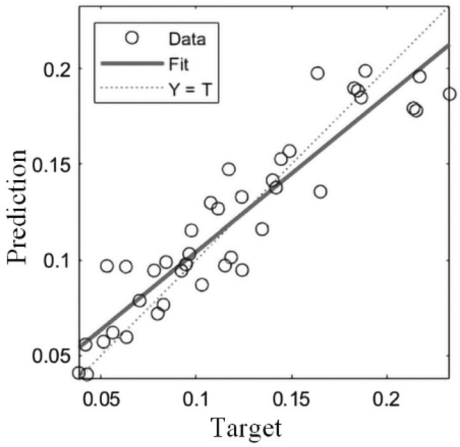

Figure 5 Regression analysis of multi-layer feedforward artificial neural network

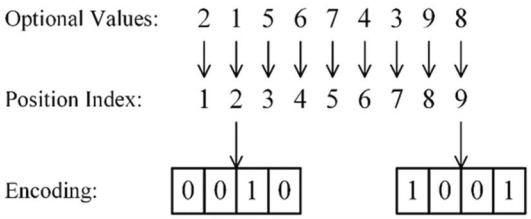

Figure 6 Position encoding

Table 6 Benchmark function specifications

Name	Formula	Dim	Decision Domain	Optimum Variable	Global Optimum
Ackley	$f(x)=-a\exp\left(-b\sqrt{\frac{1}{d}\sum_{i=1}^{d}x_i^2}\right)-\exp\left(\frac{1}{d}\sum_{i=1}^{d}\cos(cx_i)\right)+a+\exp(1)$	6	[−32.768, 2.768]	[0, ……, 0]	0
Bulkin N.6	$f(x)=100\sqrt{\lvert x_2-0.01x_1^2\rvert}+0.01\lvert x_1+10\rvert$	2	$x_1\in[-15,-5]$, $x_2\in[-3,3]$	[−10, 1]	0
Drop- Wave	$f(x)=-\frac{1+\cos\left(12\sqrt{x_1^2+x_2^2}\right)}{0.5\,(x_1^2+x_2^2)+2}$	2	[−5.12, 5.12]	[0, 0]	−1
Griewank	$f(x)=\sum_{i=1}^{d}\frac{x_i^2}{4000}-\prod_{i=1}^{d}\cos\left(\frac{x_i}{\sqrt{i}}\right)+1$	6	[−600, 600]	[0, ……, 0]	0

Table 7 Test results for comparison of MDGA and original GA

Function	Algorithm	CR	SS_{avg}	SS_{min}	SS_{max}	SS_{median}	SS_{std}
Ackley	GA	0	-	-	-		-
	MDGA	100%	90.2	29	311	64.5	69.86
Bulkin N.6	GA	0	-	-	-		-
	MDGA	100%	6.9	2	52	3	11.37
Drop-Wave	GA	25%	229	130	538	151	174.23
	MDGA	100%	7.45	2	42	4	9.65
Griewank	GA	0	-	-	-		-
	MDGA	100%	72.35	23	129	73	32.76

Note: the subscript "avg" means the average mathematical value of 20 repeated tests, "min" and "max" represent the minimum and maximum value, "median" means the median value of the results, and "std" means the standard deviation of the results

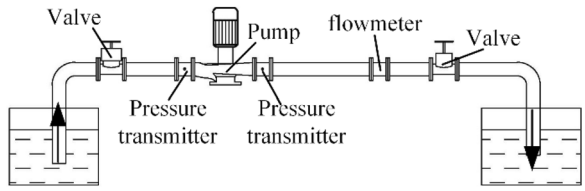

Figure 7 Test rig

Figure 8 Positions of pressure sensors

$$R^2 = 1 - \frac{\sum_{i=1}^{m} (y_i - \bar{y})^2}{\sum_{i=1}^{m} (\hat{y} - y_i)^2}, \tag{6}$$

where, m is the size of the sample set, y_i is the actual value in the sample set, $\bar{y}$ is the average mathematical value of the sample set, and $\hat{y}$ is the predicted value. The closer the value of R^2 is to 1, the higher the accuracy of the surrogate model.

2.3.2 Artificial Neural Network

An artificial neural network (ANN) is a nonlinear mathematical model of distributed parallel information processing abstracted from brain neural networks, with high fault tolerance and self-learning, self-adaptive, and associative features. ANNs are widely used in signal processing, artificial intelligence, pattern recognition, automatic control, and other research fields [31].

As mentioned in Section 1, the relationship between inner flow features and decision variables shows a strong nonlinearity, and it is hard to predict accurately. Hence, a feedforward network was applied to fix this situation to fit the relationship between PFIC and the decision variables.

Table 8 Experimental sensors specifications

Parameter	Sensor	Model	Range	Uncertainty
Inlet pressure	Pressure sensor	HM90	0-0.2MPa	±0.1%
Pressure at P2	Pressure sensor	HM90	0-0.7MPa	±0.1%
Flowrate	Turbine flowmeter	LW-80	12-120m^3/h	±0.5%
Outlet pressure	Pressure sensor	WIKA	0-1MPa	±0.1%

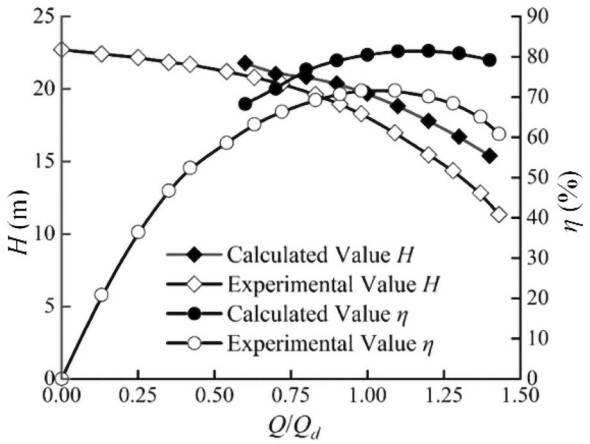

Figure 9 Comparison of performance curves

A regression analysis was also applied to ensure the stability of the trained model. The results indicated that the R^2 of the ANN obtained is 0.9303 (Figure 5), which showed great predicting precision.

2.4 Modified Discrete Genetic Algorithm

2.4.1 Modifications

Based on the classical genetic algorithm, this research proposed two main modifications: (1) position encoding and (2) adaptive genetic factors.

(1) Position Encoding

DM is defined as an n-dimensional bounded discrete space, and $\boldsymbol{M}$ represents a two-dimensional optional value array, as shown in Eq. (7):

$$\boldsymbol{M} = \begin{Bmatrix} \{val_{11}, val_{12}, \cdots, val_{1l_1}\} \\ \{val_{21}, val_{22}, \cdots, val_{2l_2}\} \\ \cdots \\ \{val_{m1}, val_{m2}, \cdots, val_{ml_m}\} \end{Bmatrix}, \tag{7}$$

where m is the number of decision variables, l_i is the number of optional values of the i-th decision variables, and val means optional value.

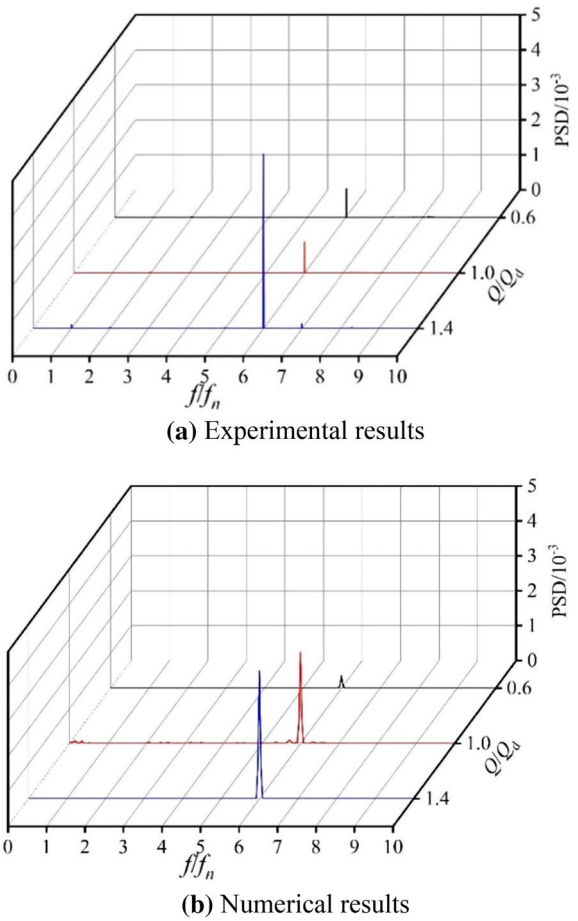

Figure 10 Comparison of pressure fluctuation results: **a** Experimental results, **b** Numerical results

That is, for the i-th decision variables, there are l_i optional values. In this research, the position index of each optional value was encoded as a binary description for further optimization. An example of the encoding logic is shown in Figure 6.

(2) Adaptive Genetic Factor

For genetic algorithms, constant crossover and mutation probabilities are executed in the preoperational stage to ensure that enough chromosomes are genetically manipulated to guarantee the diversity of the population, but this also reduces the convergence speed of the algorithm to some extent. After a certain number of iterations, adaptive genetic probabilities are used, the calculation formula of which is as follows:

$$p_c = \begin{cases} p_{c0}, f_c \geq f_{avg}, \\ p_{c0} \cdot \cos\left(\frac{f_{min} - f_c}{f_{min} - f_{avg}}\right), f_c < f_{avg}, \end{cases} \tag{8}$$

Table 9 Design variables of the original case and the optimized case

Parameter	β_2 (°)	D_2 (mm)	b_2 (mm)	θ (°)
Original case	23	136	17.8	110
Optimized case	20	133	15	120

$$p_m = \begin{cases} p_{m0}, f_m \geq f_{avg}, \\ p_{m0} \cdot \cos\left(\frac{f_{min} - f_m}{f_{min} - f_{avg}}\right), f_m < f_{avg}, \end{cases} \tag{9}$$

$$f_{avg} = \frac{\sum_{i=1}^{N} f_i}{N}, \tag{10}$$

where p_c and p_m are the adaptive crossover and mutation probabilities, respectively; p_{c0} and p_{m0} are the initial crossover and mutation probabilities, respectively; f_c is the smaller fitness value of the two chromosomes that have been paired to crossover; f_m is the fitness value of the chromosome to be mutated; f_{min} is the minimum fitness value in the population and f_{avg} is the average fitness value of the population; N is the population size; and f_i is the fitness value of the i-th chromosome.

2.4.2 Benchmark

To evaluate the performance of the MDGA, a test on four different benchmark functions was carried out with a comparison to the original genetic algorithm. The specifications of each benchmark function are listed in Table 6. The functions can be found in Refs. [32–34]. Two performance indices were utilized: convergence rate (CR) and search speed (SS). In addition, each test was repeated 20 times to ensure the reliability of the results. The maximum iteration was set to 1000, and the population size N was set to 100.

The test results are listed in Table 7. In terms of convergence rate, for each test function, MDGA achieves 100%, i.e., MDGA finds the global optimum. In comparison, only the Drop-Wave function of the GA achieves 25% convergence rate, and the other three test functions do not accurately find the theoretical optimum within the maximum number of iterations. In addition, for most cases, MDGA could converge in less than 100 iterations, which shows amazing search speed and is more suitable for the optimization problem in this research.

Table 10 Characteristic comparisons between the original case and the optimized case

Parameter	$\eta_{0.6Q_d}$	$\eta_{1.0Q_d}$	$\eta_{1.4Q_d}$	$H_{0.6Q_d}$	$H_{1.0Q_d}$	$H_{1.4Q_d}$	$C^{V1}_{0.6Q_d}$	$C^{V1}_{1.0Q_d}$	$C^{V1}_{1.4Q_d}$
Original case	67.34	79.86	77.84	21.51	19.42	15.00	0.1620	0.0887	0.0896
Optimized case	69.25	82.23	79.55	21.29	18.94	14.24	0.1649	0.0533	0.0716
Change	2.84%	2.97%	2.20%	−1.02%	−2.47%	−5.07%	1.79%	−39.91%	−20.09%

3 Experimental Validation

3.1 Test Rig Setup

To verify the rationality and accuracy of the numerical simulation, the external characteristics test and pressure fluctuation measurement test were conducted on an open test rig in the Fluid Machinery and Engineering Laboratory of Jiangsu University. The schematic diagram of the test rig is shown in Figure 7, and the pressure sensor positions are given in Figure 8. The test equipment mainly includes import and export pressure gauges and the pipeline pump, motor, frequency controller, flow meter, throttle valve, etc. The pump inlet pipeline diameter is 80 mm, and the outlet pipeline diameter is 80 mm. The specifications of the experimental sensors are listed in Table 8.

3.2 Result Comparison

A comparison between the experimental and computational results of the original case was carried out, and the results are given in Figures 9 and 10.

As shown in Figure 9, the computational and experimental results showed good agreement. For the nominal operating condition, the deviation between the computational head and the experimental head is 4.48%, and the deviation in efficiency is 4.81%. Hence, the CFD predictions had a good accuracy, which is acceptable for further use in the optimization process.

On the other hand, to facilitate the analysis of the frequency domain characteristics of the signal, the pressure fluctuation signal obtained from the experimental and numerical simulations is subjected to Fast Fourier Transform (FFT), and the Hanning window function is applied to calculate the power spectrum density (PSD). The shaft frequency $f_n = n/60 = 48.5$ Hz, and the blade passing frequency $f_{bpf} = z \times f_n = 291$ Hz. f/f_n is used to show the rotational frequency multiplier of the blade.

The main frequency of the pressure fluctuation at the monitoring point P2 under different working conditions is the blade passing frequency (BPF) because the pressure fluctuation near the tongue is mainly due to the rotor–stator interaction. As the flow rate increases, the frequency amplitude gradually increases as well. The change in the amplitude of the blade passing frequency under the small flow rate and the design flow rate was low, but the value for the overload condition rose by 578.5% compared to the design condition. Obviously, the regularity of the numerical results is consistent with the experimental results, but the amplitude prediction was not accurate enough at the nominal condition. However, the performance was good for the partial load and overload conditions.

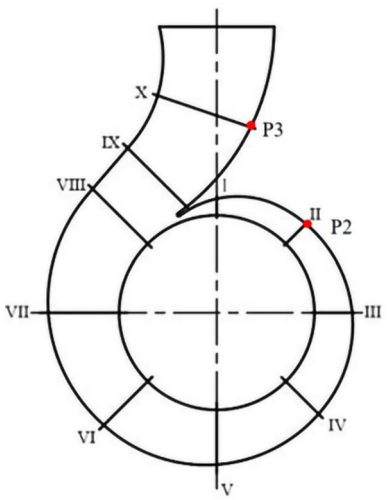

Figure 11 Schematic diagram of volute cross-sections

4 Results and Discussions

4.1 Performance Comparison

An optimization scheme with better comprehensive performance was selected based on the MDGA algorithm's search results and validated by numerical simulation for three operating conditions: $0.6Q_d$, $1.0Q_d$, and $1.4Q_d$. The design parameters between the original and optimized cases are listed in Table 9. A comparison of their performances is shown in Table 10.

The results of the optimized case predicted by the surrogate models (refer to Section 2.3) are $\hat{C}^{V1}_{p,1.0Q_d} = 0.0451$, $\hat{\eta}_{1.0Q_d} = 81.95\%$, and $\hat{H}_{1.0Q_d} = 19.53$ m. It can be found that the deviations between the predicted values and the computational values of the efficiency and the head

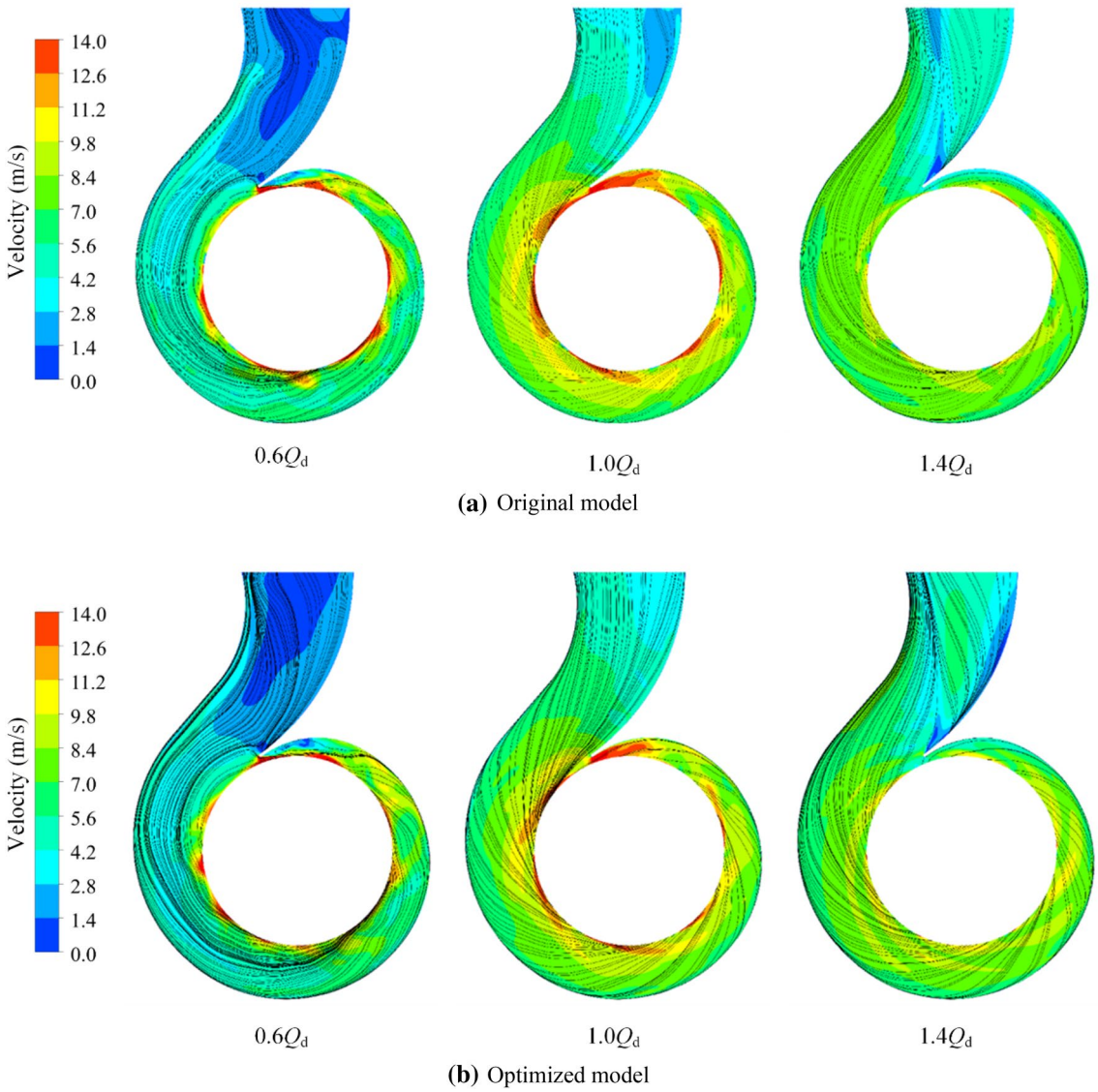

Figure 12 Velocity distribution in the volute of the original case and the optimized case: **a** Original model, **b** Optimized model

under nominal conditions are 0.35% and 3.10%, respectively, and the error for PFIC is 15.36%.

After optimization, the efficiency under all investigated conditions is improved significantly, and a maximum efficiency increase of 2.97% is obtained under the nominal condition. Compared with the original model, the optimized model has a smaller outlet blade angle, impeller outlet diameter and width, and a larger vane wrap angle. Under the selected operating conditions, the head has different degrees of reduction, and the largest head drop is found under the overload conditions, although it still meets the design requirements. In addition, the PFIC decreases significantly at the nominal and overload condition, while the difference is small for the partial load condition.

4.2 Flow Analysis

4.2.1 Volute

In order to understand the flow distribution in the volute, ten cross-sections were defined, and the positions of these sections are shown in Figure 11. Figure 12 shows the velocity distributions in the midsection of the volute for the original and optimized cases. The comparison of the PFIC distributions in the original and optimized models is illustrated in Figures 13 and 14.

For the velocity distribution (Figure 12), the flow in the spiral section of the volute is more uniform, and the

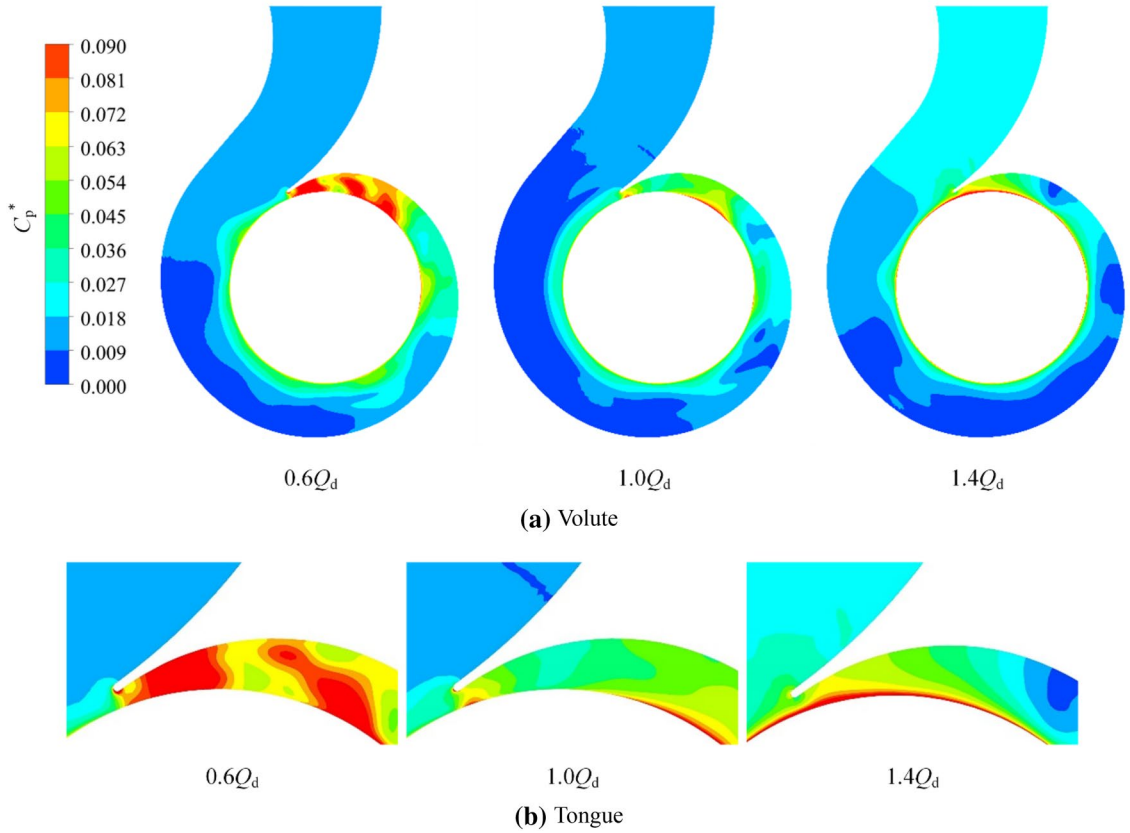

Figure 13 PFIC distribution in the volute of the original case: **a** Volute, **b** Tongue

changes are mainly concentrated in the diffusion tube under the partial load condition. In the original model, the low-velocity area in the diffusion tube is larger, which changes slightly after optimization. Moreover, the flow distribution became more uniform and the velocity in the mainstream area increased slightly after optimization. For the nominal condition, the flow separation can be observed in the diffusion tube of the original model, which disappears after optimization, and the near-wall velocity decreases. In the overload condition, a small area of flow separation is found on the outside of the tongue, which is improved after optimization, and the velocity in the mainstream area increases.

As shown in Figures 13 and 14, under the partial load condition, the high PFIC region is mainly concentrated in the area near section II, and the highest PFIC was found near the inner side of the tongue. After optimization, the PFIC at the volute inlet and near the tongue is significantly reduced due to the decrease in the working capacity of the impeller. Meanwhile, the PFIC gradient is reduced, and the high PFIC area also becomes smaller after optimization. Similarly, for the nominal condition, the PFIC near the interface and tongue decreases dramatically after optimization, the high PFIC region around the tongue nearly disappears, and a more uniform pressure distribution is achieved. Under the overload condition, the overall PFIC in the volute decreases after optimization, and the low PFIC area between sections II and III decreases greatly compared with the original case.

4.2.2 Impeller

The comparison of the velocity distribution on the impeller's middle plane between the original case and the optimized case is given in Figure 15, and the comparison of the PFIC distribution is shown in Figure 16.

It can be seen from Figure 15 that the flow condition was extremely complicated under the partial load condition. Serious flow separations could be observed on the suction side of the blade. In addition, the recirculation could be found near the impeller outlet, which resulted in the vortices at the suction side and blocked the passage. After optimization, this phenomenon was improved due to the drop in pressure in the volute. For the nominal and overload conditions, the velocity gradient in the impeller

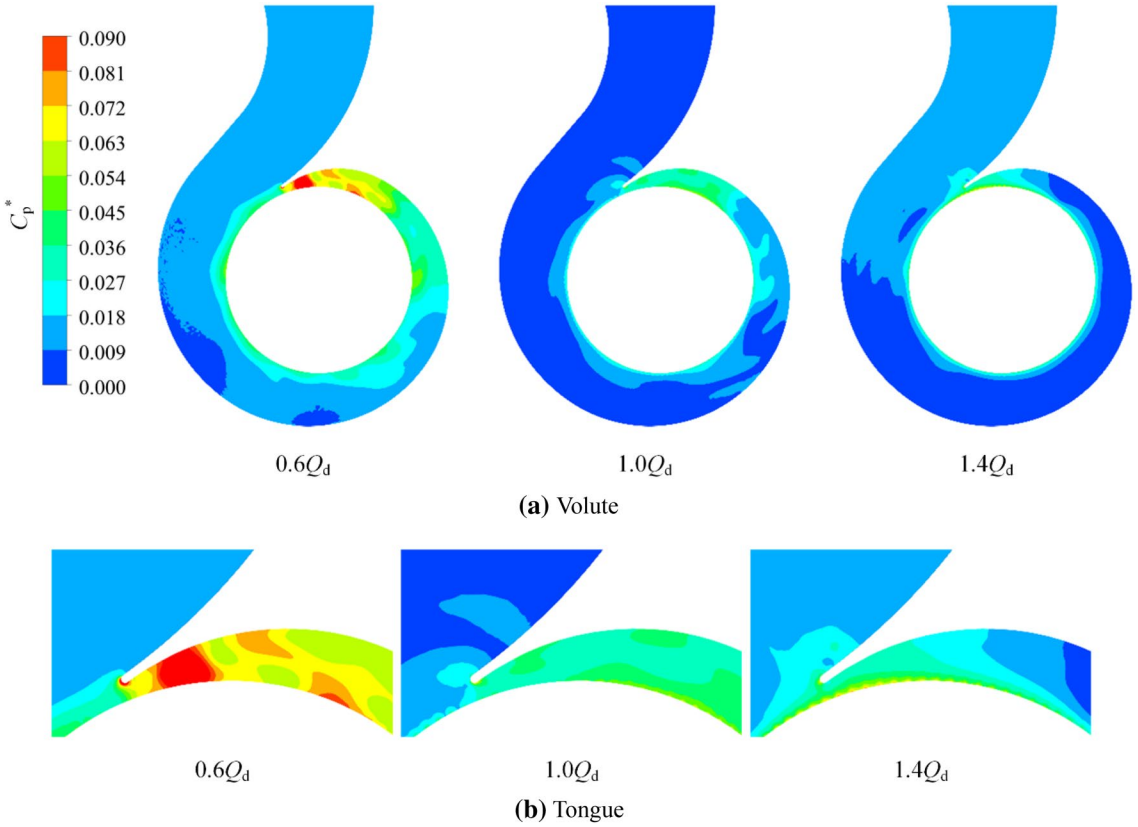

Figure 14 PFIC distribution in the volute of the optimized case: **a** Volute, **b** Tongue

decreased, and a uniform velocity distribution can be observed after optimization.

From Figure 16, the PFIC increased from the inlet to the outlet because of the work of the impeller. The low PFIC region was concentrated on the inlet of the impeller. The highest value and the gradient for the PFIC were dropped after optimization, especially for the partial load condition, mainly due to the improvement in the flow distribution. In addition, the low PFIC region in the impeller greatly increased after optimization under both the nominal and the overload conditions.

5 Conclusions

In this research, design optimization of the impeller of the inline pump was carried out to improve the efficiency and working stability based on the transient database. After the data-mining process, four design variables were chosen as the decision variables, and 40 sample cases were generated and calculated by the automatic simulation program in the unsteady state. On the other hand, a modified discrete genetic algorithm was proposed to reduce the optimization cost. The accuracy of the simulation, considering both pump performance and pressure fluctuation, was verified. Finally, a great improvement in performance was obtained after optimization. The main conclusions of this research are given as follows.

(1) The cost of optimization to improve the unsteady characteristics (i.e., PFIC) of pumps is obviously more expensive than the optimization of steady features (i.e., efficiency), and this problem will be tough to solve if the number of decision variables is large.
(2) The accuracy of the simulation is proven to be extraordinarily coincidental with the experiment. The dominant frequency and the tendency for the pressure fluctuations to vary are the same in the experiments and simulations.
(3) The surrogate model fits the relationship between external characteristics and design parameters. The R^2 of the ANN is 0.9303, showing great prediction precision. However, its prediction for the internal flow features is still not efficient.

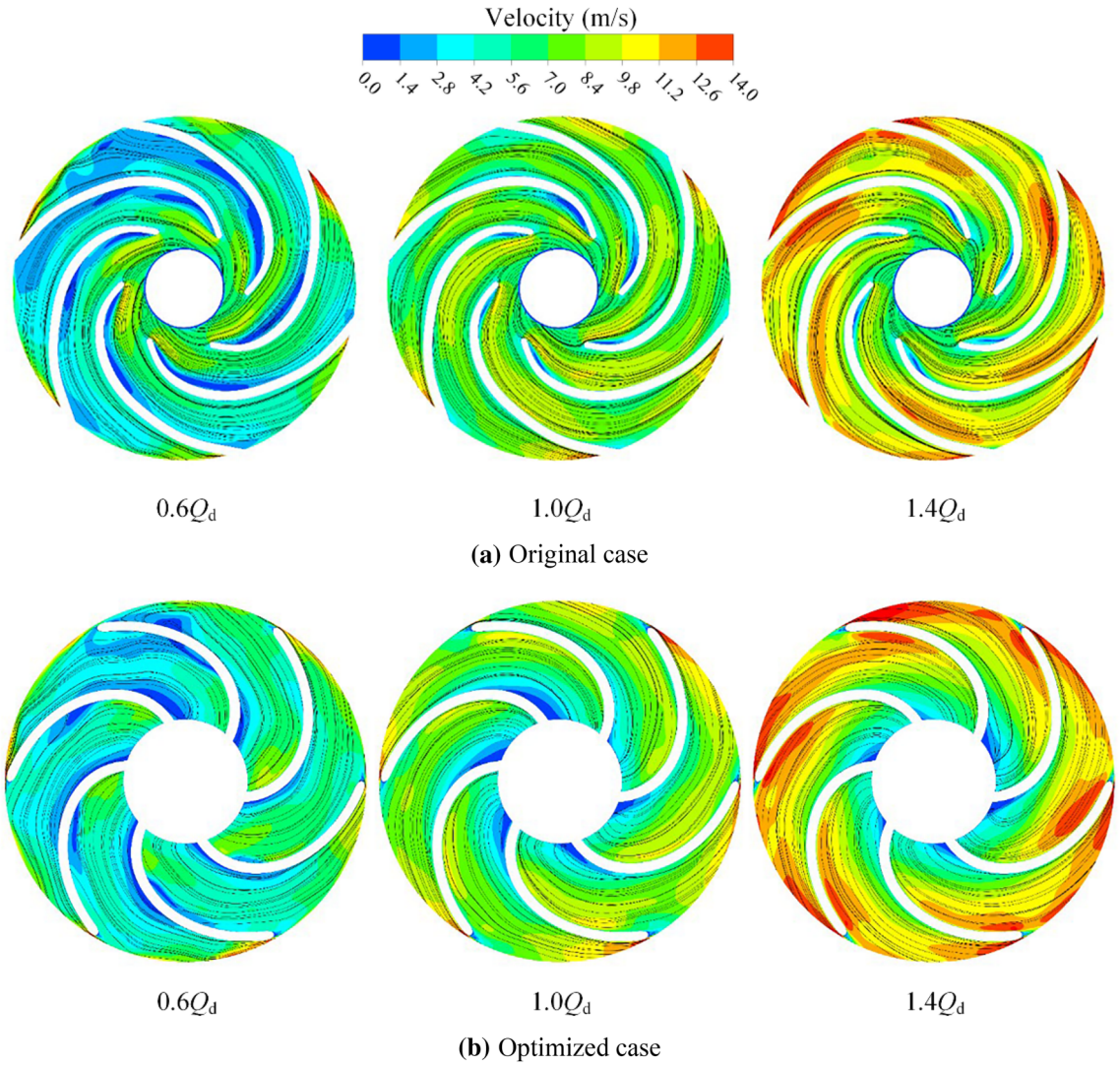

Figure 15 Velocity distributions in the impeller of the original case and the optimized case: **a** Original model, **b** Optimized model

(4) The proposed MDGA has significant advantages over the original GA in terms of its search speed and convergence rate. MDGA increases the convergence rate from 25% to 100% for the Drop-Wave function. The convergence rate is also 100% for the Ackley, Bulkin N.6, and Griewank functions, where the GA fails to find the optimum accurately within the maximum number of iterations.

(5) The performance and stability of the inline pump were significantly improved after optimization. The efficiency is greatly enhanced, increasing by more than 2.2%, while the pump head drops slightly. The pressure fluctuation intensity coefficient drops more than 20% under nominal and $1.4Q_d$ conditions but increases by 1.79% under the $0.6Q_d$ condition.

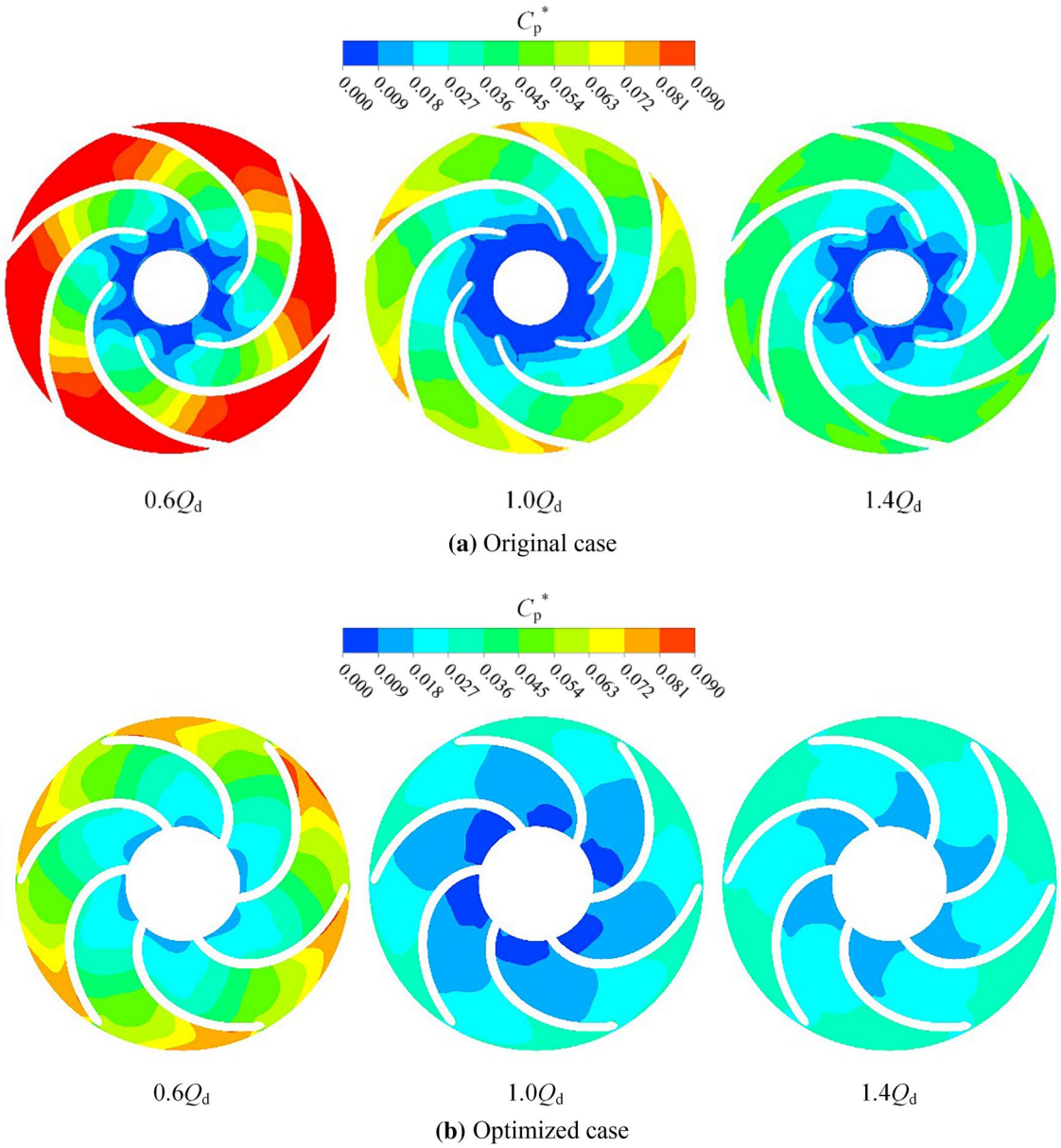

Figure 16 PFIC distribution in the impeller of the original case and the optimized case: **a** Original model, **b** Optimized model

Acknowledgements
The authors sincerely thanks to 4C-Pump R&D Group for supporting the experimental test and computational source.

Author contributions
WW and JP were in charge of the whole trial; WW and QD wrote the manuscript; JC and XG assisted with sampling and laboratory analyses. All authors read and approved the final manuscript.

Authors' Information
Wenjie Wang, born in 1990, is currently an associate researcher at *Jiangsu University, China*. He received his PhD degree from *Jiangsu University, China*, in 2018. His research interests include intelligent optimization algorithm improvement, hydraulic optimization design of fluid machinery, measurement and analysis of unsteady flow in pumps, and transient flow characteristics of pump turbine.
Qifan Deng, born in 1994, is currently a PhD candidate at *National Research Center of Pumps, Jiangsu University, China*. He received his master degree from *Jiangsu University, China*, in 2020. His research interests include pump optimization and unstable flow in pump.
Ji Pei, born in 1984, is currently a researcher at *Jiangsu University, China*. He received his PhD degree from *Jiangsu University, China*, in 2013. His research interests include fluid machinery (pump) advanced optimization design method, internal flow theory, and multidisciplinary coupling analysis.
Jinwei Chen, born in 1995, is currently an operator at *CHN Energy Jiangsu Jianbi Power Co., Ltd., China*. She received her master's degree from *Jiangsu University, China*, in 2021. She is mainly engaged in the itinerant inspection and operator of power plant equipment and systems.

Xingcheng Gan, born in 1994, is currently an assistant researcher at *Jiangsu University, China*. He received his Ph.D. degree from *Jiangsu University, China*, in 2023. His research interests include hydraulic optimization for fluid machinery, swarm intelligence, and energy-saving optimization for pump systems.

Funding
Supported by National Key Research and Development Program of China (Grant No. 2022YFC3202901), Natural Science Foundation of China (Grant No. 51879121), Jiangsu Provincial Primary Research & Development Plan (Grant No. BE2019009-1), and China Scholarship Council (Grant No. 202108690020).

Data availability
Data will be made available on request.

Declarations

Competing Interests
The authors declare no competing financial interests.

Received: 8 November 2021 Revised: 4 July 2023 Accepted: 10 July 2023
Published online: 31 July 2023

References

[1] C Stephen, S Yuan, J Pei, et al. Numerical flow prediction in inlet pipe of vertical inline pump. *Journal of Fluids Engineering*, 2018, 140(5): 051201.
[2] S Chu, R Dong, J Katz. Relationship between unsteady flow, pressure fluctuations, and noise in a centrifugal pump—Part B: effects of blade-tongue interactions. *Journal of Fluids Engineering*, 1995, 117(1): 30-35.
[3] Z Wang, Z Qian, J Lu, et al. Effects of flow rate and rotational speed on pressure fluctuations in a double-suction centrifugal pump. *Energy*, 2019, 170: 212-227.
[4] D Fu, F Wang, P Zhou, et al. Impact of impeller stagger angles on pressure fluctuation for a double-Suction centrifugal pump. *Chinese Journal of Mechanical Engineering*, 2018, 31(1): 198-211.
[5] D Li, Y Qin, J Wang, et al. Optimization of blade high-pressure edge to reduce pressure fluctuations in pump-turbine hump region. *Renewable Energy*, 2022, 181: 24-38.
[6] A A El-Hadj, S Abd Rahim. Optimization of an external gear pump using response surface method. *Journal of Mechanics*, 2020, 36(4): 567-575.
[7] X Gan, J Pei, W Wang, et al. Multi-component optimization of a vertical inline pump based on multi-objective PSO and artificial neural network. *Journal of Mechanical Science and Technology*, 2020, 34: 4883-4896.
[8] Z Sun, S Xiao, M Xu, et al. Optimization of the structure of water axial piston pump and cavitation of plunger cavity based on the Kriging model. *Journal of Vibroengineering*, 2016, 18(4): 2460-2474.
[9] W Wang, S Yuan, J Pei, et al. Optimization of the diffuser in a centrifugal pump by combining response surface method with multi-island genetic algorithm. *Proceedings of the Institution of Mechanical Engineers Part E: Journal of Process Mechanical Engineering*, 2017, 231(2): 191-201.
[10] Z Li, X Zheng. Review of design optimization methods for turbomachinery aerodynamics. *Progress in Aerospace Sciences*, 2017, 93: 1-23.
[11] J Madsen, W Shyy, R Haftka. Response surface techniques for diffuser shape optimization. *AIAA Journal*, 2000, 38: 1512-1518.
[12] X Gan, J Pei, S Yuan, et al. Multi-objective optimization on inlet pipe of a vertical inline pump based on genetic algorithm and artificial neural network. *ASME 2018 5th Joint US-European Fluids Engineering Division Summer Meeting*, Montreal, Quebec, Canada, July 15–20, 2018: 51555: V001T06A003.
[13] W Wang, M Osman, J Pei, et al. Artificial neural networks approach for a multi-objective cavitation optimization design in a double-suction centrifugal pump. *Processes*, 2019, 7(5): 246.
[14] J Kim, J Choi, K Kim. Design optimization of a centrifugal compressor impeller using radial basis neural network method. *ASME Turbo Expo 2009: Power for Land, Sea, and Air*, Orlando, Florida, USA, June 8–12, 200: 443-451.
[15] Y Zhang, S Hu, J Wu, et al. Modeling and multi-objective optimization of double suction centrifugal pump based on kriging meta-models. *Advances in Global Optimization*, 2015, 95: 251-261.
[16] J Pei, W Wang, M Osman, et al. Multiparameter optimization for the nonlinear performance improvement of centrifugal pumps using a multi-layer neural network. *Journal of Mechanical Science and Technology*, 2019, 33: 2681-2691.
[17] A Demeulenaere, A Ligout, C Hirsch. Application of multipoint optimization to the design of turbomachinery blades. *ASME Turbo Expo 2004: Power for Land, Sea, and Air*, Vienna, Austria, June 14–17, 2004:1481-1489.
[18] X Gan, W Wang, J Pei, et al. Direct shape optimization and parametric analysis of a vertical inline pump via multi-objective particle swarm optimization. *Energies*, 2020, 13(2): 425.
[19] R Huang, X Luo, B Ji, et al. Multi-objective optimization of a mixed-flow pump impeller using modified NSGA-II algorithm. *Science China-Technological Sciences*, 2015, 58: 2122-2130.
[20] S Dhanalakshmi, S Kannan, K Mahadevan, et al. Application of modified NSGA-II algorithm to combined economic and emission dispatch problem. *International Journal of Electrical Power & Energy Systems*, 2011, 33: 992-1002.
[21] F Miao, H Park, C Kim, et al. Swarm intelligence based on modified PSO algorithm for the optimization of axial-flow pump impeller. *Journal of Mechanical Science and Technology*, 2015, 29: 4867-4876.
[22] A Nourbakhsh, H Safikhani, S Derakhshan. The comparison of multi-objective particle swarm optimization and NSGA II algorithm: applications in centrifugal pumps. *Engineering Optimization*, 2011, 43: 1095-1113.
[23] J Holland. *Adaptation in natural and artificial systems: an introductory analysis with applications to biology, control, and artificial intelligence*. Cambridge: MIT press, 1992.
[24] S Derakhshan, M Pourmahdavi, E Abdolahnejad, et al. Numerical shape optimization of a centrifugal pump impeller using artificial bee colony algorithm. *Computers & Fluids*, 2013, 81:145-151.
[25] M Namazizadeh, M Gevari, M Mojaddam, et al. Optimization of the splitter blade configuration and geometry of a centrifugal pump impeller using design of experiment. *Journal of Applied Fluid Mechanics*, 2020, 13: 89-101.
[26] M Wang, Y Li, J Yuan, et al. Comprehensive improvement of mixed-flow pump impeller based on multi-objective optimization. *Processes*, 2020, 8(8): 905.
[27] J Pei, T Yin, S Yuan, et al. Cavitation optimization for a centrifugal pump impeller by using orthogonal design of experiment. *Chinese Journal of Mechanical Engineering*, 2017, 30: 103-109.
[28] ANSYS. *ANSYS CFX User's Guide, Release 20.2*. Canonsburg, USA: ANSYS Inc, 2019.
[29] H Shim, K Kim. Evaluation of rotor–stator interface models for the prediction of the hydraulic and suction performance of a centrifugal pump. *Journal of Fluids Engineering*, 2019, 141(11): 111106.
[30] A Khuri, S Mukhopadhyay. Response surface methodology. *Wiley Interdisciplinary Reviews: Computational Statistics*, 2010, 2: 128-149.
[31] Z Zhang. Artificial neural network// *Zhihua Zhang*. *Multivariate time series analysis in climate and environmental research*. Cham: Springer, 2018: 1-35.
[32] S Lim, H Haron. Performance comparison of genetic algorithm, differential evolution and particle swarm optimization towards benchmark functions. *2013 IEEE Conference on Open Systems*, Kuching, Malaysia, 2013: 41-46.
[33] M Alavidoost, M Tarimoradi, MHF Zarandi. Fuzzy adaptive genetic algorithm for multi-objective assembly line balancing problems. *Applied soft computing*, 2015, 34: 655-677.
[34] E Haq, I Ahmad, A Hussain, et al. A novel selection approach for genetic algorithms for global optimization of multimodal continuous functions. *Computational Intelligence and Neuroscience*, 2019: 1-14.